Asian Journal of Chemistry; Vol. 38, No. 5 (2026), 1127-1134
ASIAN JOURNAL OF CHEMISTRY
https://doi.org/10.14233/ajchem.2026.35552

Structural, Kinetic and Thermodynamic Analysis of Cellulose Contents Extracted from *Sericostoma pauciflorum*

JITUBHAI MORABIYA[1,*], HARDIK BHATT[2] and SANJAY BAMANIYA[1]

[1]Department of Chemistry, Bhakta Kavi Narsinh Mehta University, Junagadh-362263, India
[2]Department of Chemistry, SET Science College and P.G. Centre, Junagadh-362001, India

*Corresponding author: E-mail: jitubhamorabiya@gmail.com

Received: 31 December 2025 *Accepted*: 28 February 2026 *Published online*: 4 May 2026 AJC-22336

In this study, cellulose was extracted from *Sericostoma pauciflorum*, a commonly plant found in Gujarat state of India. The extracted material was further fractionated into crude cellulose, α-cellulose and β-cellulose, and these fractions were characterised by SEM, FTIR, XRD and TGA to evaluate their surface morphology, chemical composition, crystallinity and thermal stability. SEM images showed that α-cellulose had a clear fibrous structure, while β-cellulose appeared flaky and clustered, indicating lower crystallinity. FTIR and XRD results confirmed the successful removal of lignin and hemicellulose and showed that α-cellulose possessed higher crystallinity. Thermal degradation behaviour was studied using TGA and kinetic parameters were calculated using the Coats-Redfern method with a 21 solid-state reaction model. The DM06 (Zhuravlev equation) model was most suitable for crude and β-cellulose, whereas the NM 04 (Avrami-Erofeev, n = 2) model best explained the decomposition of α-cellulose. Thermodynamic analysis showed positive enthalpy and Gibb's free energy values, indicating that the pyrolysis process is endothermic and non-spontaneous.

Keywords: *Sericostoma pauciflorum*, α-Cellulose, β-Cellulose, Fractionation, Acid-alkali treatment.

INTRODUCTION

The growing need for eco-friendly materials and renewable energy has led to increased worldwide research on polymers derived from biomass. Among these materials, cellulose is the most plentiful natural biopolymer on earth and is commonly found in plant cell walls and agricultural waste [1]. Due to its renewable, biodegradable, non-toxic and mechanically robust nature, cellulose is widely used in paper, textile, composite, pharmaceutical and bioenergy industries [2]. In recent times, it has also attracted attention as an important raw material for advanced functional materials, carbon-based products and biofuels [3]. Structurally, cellulose is a linear polysaccharide made up of β–(1→4)-linked D-glucose units that form long chains held together by intra- and intermolecular hydrogen bonds [4,5]. Based on the polymerisation degree, crystallinity and alkaline solubility, cellulose is classified into α-, β- and γ-fractions, where α-cellulose possesses high molecular weight and crystallinity with alkali insolubility, while β-cellulose consists of partially degraded chains with lower structural order [6-8]. The proportion and characteristics of these different cellulose fractions play an important role in determining their thermal behaviour, chemical reactivity and suitability for various applications. The way cellulose breaks down when heated is a key factor in its use for energy production and materials conversion [9].

Thermogravimetric analysis (TGA) is commonly used to evaluate the thermal stability and decomposition behaviour of cellulose; however, kinetic modelling is essential to determine key parameters such as activation energy and pre-exponential factor, which provide insight into degradation mechanisms and reaction pathways [10-12]. Model-free isoconversional methods including Flynn-Wall-Ozawa (FWO), Kissinger-Akahira-Sunose (KAS), Friedman & Vyazovkin approaches [12,13], estimate the activation energy at different conversion levels without assuming a specific reaction model, thereby reducing model bias. Distributed activation energy models are also applied to describe complex multistep decomposition behaviour of lignocellulosic materials [14].

Among model-fitting techniques, the Coats-Redfern method remains widely used for solid-state reactions [15], allowing estimation of kinetic parameters by testing different reaction

This is an open access journal, and articles are distributed under the terms of the Attribution 4.0 International (CC BY 4.0) License. This license lets others distribute, remix, tweak, and build upon your work, even commercially, as long as they credit the author for the original creation. You must give appropriate credit, provide a link to the license, and indicate if changes were made.

models and identifying the most suitable mechanism [16,17]. In addition, thermodynamic parameters such as enthalpy change (ΔH), entropy change (ΔS) and Gibbs free energy change (ΔG) provide information on energy requirements, reaction feasibility and structural disorder during cellulose pyrolysis [18,19].

In this work, *Sericostoma pauciflorum* (Karvas), a widely available plant from the Junagadh district of Gujarat, India, was selected as a sustainable biomass source for cellulose extraction. Despite its abundance, this species has received limited attention for cellulose recovery and value addition. Utilizing such locally available biomass can reduce dependence on wood-based sources while supporting waste minimization and circular bio-economy practices. Accordingly, crude cellulose was extracted, fractionated into α- and β-cellulose and systematically characterized for structural, morphological and thermal properties. Furthermore, kinetic and thermodynamic analyses using the Coats-Redfern method were performed to understand the degradation behaviour and energy requirements of the cellulose fractions, highlighting the potential of *S. pauciflorum* as a sustainable source for advanced applications.

EXPERIMENTAL

Sericostoma pauciflorum, locally called Karvas, is widely found in the Junagadh District (21.3551º N, 70.5265º E) of Gujarat state, India. Fresh, healthy plants were collected from the forest areas of Junagadh between May and July 2024. Methanol was mainly used to remove pigments during the cellulose purification process. Other chemicals such as sodium acetate, sodium chlorite, sodium hydroxide, sodium hypochlorite, and sulphuric acid were used at different stages to remove lignin, hemicellulose and other unwanted substances. All chemicals and solvents used were of analytical grade and purchased from Sisco Research Laboratory (SRL), Mumbai, India, unless specified

Isolation of cellulose: Cellulose was extracted from *S. pauciflorum* using the method described by Parihar *et al.* [20]. Fresh plant samples were first washed thoroughly with clean distilled water to remove dust, soil and surface impurities. The cleaned samples were shade-dried, ground into fine powder and defatted using methanol (500 mL) at room temperature for eight days to remove waxes and fats. The defatted material was bleached with sodium chlorite in acetate buffer at 60 ºC for 3 h, washed to neutrality and treated with 0.5 M NaOH at 60 ºC overnight to remove hemicellulose and non-cellulosic components. The alkali-treated sample was filtered, washed and further treated with 5% HCl under gentle boiling, followed by standing overnight, filtration, washing and drying to obtain purified cellulose.

Fractionation of cellulose: Fractionation of α- and β-cellulose from crude cellulose was carried out according to Parihar *et al*. [20]. Crude cellulose was treated with 17.5% NaOH at 20 ºC for 2 h with continuous stirring, resulting in insoluble α-cellulose and dissolved β-cellulose. The mixture was centrifuged, the residue collected as α-cellulose and β-cellulose was recovered by acid precipitation of the supernatant using 3 N H_2SO_4 at 80 ºC. The obtained fractions were washed, freeze-dried and used for yield determination.

Characterisation: The isolated cellulose fractions (crude, α- and β-cellulose) were systematically characterised using SEM, FTIR, XRD and TGA techniques. SEM (Hitachi SU-8010) was used to study surface morphology, while FTIR (Shimadzu IRAffinity-1) confirmed the presence of the functional groups and the removal of lignin and hemicellulose. XRD (Empyrean, Malvern Panalytical) was employed to determine crystallinity within the 2θ range of 5º-80º. Thermal degradation behaviour was analysed using TGA (NETZSCH Libra TGA 209 F1) under nitrogen at 10 Km min^{-1} and the Coats-Redfern method was applied to evaluate the kinetic and thermodynamic parameters. The universal form of the Coats-Redfern equation is shown in eqn. 1 [21]:

$$\ln\left[\frac{g(\alpha)}{T^2}\right] = \ln\left[\frac{AR}{\beta E_a}\right]\left(1-\frac{2RT}{E_a}\right) - \frac{E_a}{RT} \quad (1)$$

here, assuming that $2RT/E_a < 1$, the term is neglected in eqn. 1 and the expression is rearranged to obtain eqn. 2, as shown below:

$$\ln\left[\frac{g(\alpha)}{T^2}\right] = \ln\left[\frac{AR}{\beta E_a}\right] - \frac{E_a}{RT} \quad (2)$$

where g(α) signifies the numerous kinetic modal functions; β is the the heating rate (ºC min^{-1}); R is the gas constant (0.008321 kJ mol^{-1}); T is a temperature in Kelvin; and A is a frequency factor (min^{-1}); α is the degree of transformation of the sample, which was calculated using eqn. 3:

$$\alpha = \frac{M_o - M_i}{M_o - M_f} \quad (3)$$

where M_o = the mass value at t = 0, M_i = instantaneous mass value at any time and M_f = the final mass value of the individual sample. The activation energy (E_a) and frequency factor (A) were studied by plotting $\ln[g(\alpha)/T^2]$ against 1/T, as mentioned in eqn. 2. The slope achieved as a linear plot has approximate similarities to $-E_a/RT$, while the intercept has an approximation to the $\ln [AR/\beta E_a]$.

The reaction mechanism models [g(α)] are listed in Table- 1 and the activation energy and frequency factor were determined from the slope and intercept of the corresponding regression lines. In this study, 21 reaction mechanism models were examined to evaluate the kinetic and thermodynamic parameters, as presented in Table-1.

The thermodynamic parameters were calculated from the kinetic parameters using eqns. 4-6, which were employed to derive these values [15].

Change in enthalpy:

$$\Delta H = E_a - RT \quad (4)$$

Gibbs free energy:

$$\Delta G = \Delta H - T\Delta S \quad (5)$$

Entropy:

$$\Delta S = R \ln\left(\frac{Ah}{K_R T}\right) \quad (6)$$

TABLE-1
TWENTY-ONE REACTION MECHANISM MODELS [g(α)] OF COATS-REDFERN METHOD [22]

S. No.	g(α)	Model code	Models
1	α	CRO 0	Zero-order reaction (n=0)
2	-ln[1–α]	CRO 1	First-order reaction (n=1)
3	$2[(1-\alpha)^{-1.5}-1]$	CRO 1.5	One and a half order reaction (n=1.5)
4	[1/(1–α)]–1	CRO 2	Second-order reaction (n=2)
5	$0.5[(1-\alpha)^{-2}-1]$	CRO 3	Third-order reaction (n=3)
6	α^2	DM 1	Parabolic law-one-way transport
7	(1–α)–ln(1–α)+α	DM 2	Two-way transport
8	$[[-\ln(1-\alpha)]^{1/3}]^2$	DM 3	Three-way transport
9	α + (1–α)ln(1–α)	DM 4	Valensi equation (2D diffusion)
10	$(1-2\alpha/3)-(1-\alpha)^{2/3}$	DM 5	Ginstling–Brounshtein equation (anti-Jander equation)
11	$[(1-\alpha)^{-1/3}-1]^2$	DM 6	Zhuravlev equation
12	$[1-(1-\alpha)^{1/3}]^2$	DM 7	Jander equation
13	$1-(0.67\alpha)-(1-\alpha)^{0.67}$	DM 8	Ginstling equation
14	$1-(1-\alpha)^{1/2}$	GM 1	Cylindrical shape
15	$1-(1-\alpha)^{1/3}$	GM 2	Sphere shape
16	$\alpha^{1/2}$	NM 1	Power law(P2)
17	$\alpha^{1/3}$	NM 2	Power law (P3)
18	$\alpha^{1/4}$	NM3	Power law (P4)
19	$[-\ln(1-\alpha)]^{1/2}$	NM 4	Avramie-Erofeev equation (n = 2)
20	$[-\ln(1-\alpha)]^{1/3}$	NM 5	Avramie-Erofeev equation (n =3)
21	$[-\ln(1-\alpha)]^{2/3}$	NM 6	Avramie-Erofeev equation (n = 2/3)

CRO = Chemical reaction model, DM = diffusion model, GM = geometric model, NM = Random nucleation and nuclei growth

RESULTS AND DISCUSSION

The extraction process yielded 82% crude cellulose from *Sericostoma pauciflorum*, which was further fractionated into 83.6% α-cellulose and 8.2% β-cellulose. These findings indicate that α-cellulose is a major component, while β-cellulose occurs only in small quantities. The crude cellulose yield was calculated based on the mass of defatted plant residue following the method described by Parihar *et al.* [20], the percentage yield was calculated using eqn. 7:

$$\text{Crude cellulose (\%)} = \frac{M_{crude}}{M_{residue}} \times 100 \quad (7)$$

where M_{crude} = obtained crude cellulose mass, $M_{residue}$ = defatted *Sericostoma Pauciflorum* plant residue. While the % yield of α- and β-cellulose was determined by the amount of crude cellulose using eqns. 8 and 9, respectively.

$$\alpha\text{-Cellulose (\%)} = \frac{M_{\alpha}}{M_{crude}} \times 100 \quad (8)$$

$$\beta\text{-Cellulose (\%)} = \frac{M_{\beta}}{M_{crude}} \times 100 \quad (9)$$

where M_{α} = α-cellulose mass, M_{β} = β-cellulose mass.

FTIR spectral studies: FTIR spectra of crude cellulose, α-cellulose and β-cellulose show significant structural variations based on their functional group vibrations (Fig. 1). All samples display a broad absorption band around ≈ 3500-3340 cm^{-1}, which is related to O-H stretching vibrations and indicates the presence of intra- and intermolecular hydrogen bonding typical of cellulose [20]. Crude cellulose shows reduced peak intensity due to interference from remaining lignin and hemicellulose. The peaks observed in 2920-2850 cm^{-1} region

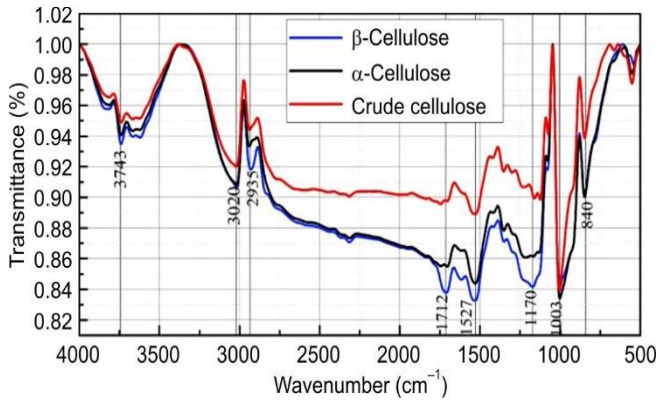

Fig. 1. FTIR spectra of crude cellulose (b) α-cellulose and (c) β-cellulose

correspond to the C-H stretching of aliphatic groups and are sharper in purified α-cellulose and β-cellulose, indicating better removal of non-cellulosic materials [22]. A distinct peak at approximately 1730 cm^{-1}, visible in crude cellulose but absent in α-cellulose, is associated with C=O stretching from hemicellulose or lignin, confirming effective purification of α-cellulose [23]. The fingerprint region between 1500-900 cm^{-1} shows well-defined peaks for both α-cellulose and β-cellulose. The band near 1427 cm^{-1}, linked to CH bending and crystallinity, is stronger in α-cellulose, indicating higher crystallinity order [24]. The peaks at 1160 cm^{-1} (C-O-C *str.*) and 1050-1030 cm^{-1} (C-O *str.* in pyranose rings) are more intense in α-cellulose. A small peak near 840 cm^{-1} confirms the presence of β-glycosidic linkages, displaying that the cellulose backbone remains intact [24]. Thus, FTIR results clearly indicate that α-cellulose is present in the crystalline form, β-cellulose has moderate structural order, whereas crude cellulose contains impurities.

Morphological studies: The first and third images of SEM (Fig. 2a,c) show that the material has a distinctly fibrous and thread-like structure. The SEM images clearly show structural differences between α-cellulose and β-cellulose. The microstructure of α-cellulose consists of long, continuous and well-connected microfibrils, which is a typical feature of highly crystalline cellulose. In contrast, the SEM image of β-cellulose reveals a very different morphology. Instead of elongated fibers, it contains compact, flaky and aggregated sheet-like particles. These features represent the less crystalline and more amorphous part of cellulose that forms due to the chemical treatment. The collapsed and flaky structure suggests shorter polymer chains and weaker bonding between fibrils. This clear difference between fibrous α-cellulose and aggregated β-cellulose supports the experimental yield results, confirming that α-cellulose is the major and more structurally stable fraction in *S. pauciflorum.*

XRD studies: XRD patterns of crude cellulose, α- and β-cellulose (Fig. 3) show clear differences in crystallinity, purity and structural organisation. Crude cellulose displays a broad and less intense diffraction peak around $2\theta \approx 22^{o}$, which corresponds to the (002) crystalline plane of crude cellulose, indicating lower crystallinity [24]. In contrast, β-cellulose shows several sharp and intense diffraction peaks across the 2θ range, with a prominent peak near $2\theta \approx 30^{o}$. The presence of multiple sharp peaks suggests that β-cellulose may contain inorganic impurities, crystalline salts or reprecipitated materials formed during processing. The diffractogram of α-cellulose shows a strong, sharp and well-defined peak at $2\theta \approx 22^{o}$, along with moderate peaks at lower angles. The increased sharpness and intensity of this main peak indicate a higher level of crystallinity and effective removal of amorphous components during purification. When compared with crude cellulose and β-cellulose, α-cellulose exhibits the most ordered cellulose structure, confirming its higher purity and better structural uniformity.

Thermal studies: The TGA curves illustrate the thermal degradation behaviour of different cellulosic fractions (Fig. 4a-c). All samples show an initial weight loss below 150 ºC due to moisture evaporation and removal of physically adsorbed water. Crude cellulose undergoes multiple decomposition stages including a minor weight loss between 100-200 ºC caused by bound water and volatile impurities, followed by major degradation (about 59%) between 250-400 ºC due to the breakdown of hemicellulose, lignin residues and cellulose. α-Cellulose exhibits the lowest initial mass loss (~3.9%) and shows a slower, more stable degradation pattern. Its main decomposition (23%) occurs between 300-380 ºC, indicating higher purity and crystallinity. In comparison, β-cellulose shows a higher early weight loss (around 11%) and the greatest primary degradation (about 64%), reflecting its lower structural order and higher amorphous content. Beyond 500 ºC, only a small char residue remains for all samples and α-cellulose produces the minimum residue.

Kinetic studies: The kinetic behaviour of various cellulosic fractions was thoroughly examined using the Coats-Redfern integral approach. A total of 21 solid-state reaction models were applied and classified into four main groups to

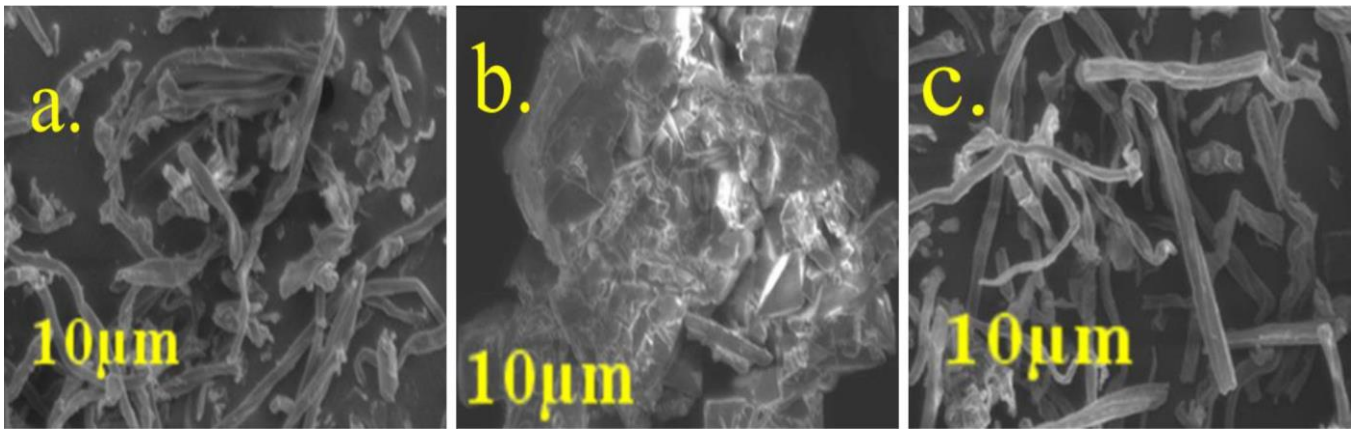

Fig. 2. SEM images (a) crude cellulose (b) α-cellulose and (c) β-cellulose

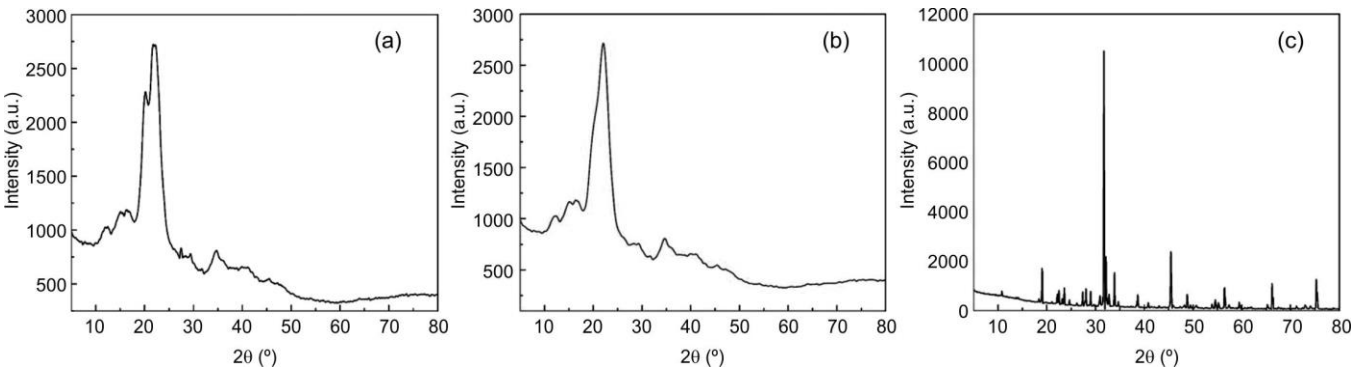

Fig. 3. XRD spectra of (a) crude cellulose, (b) α-cellulose and (c) β-cellulose

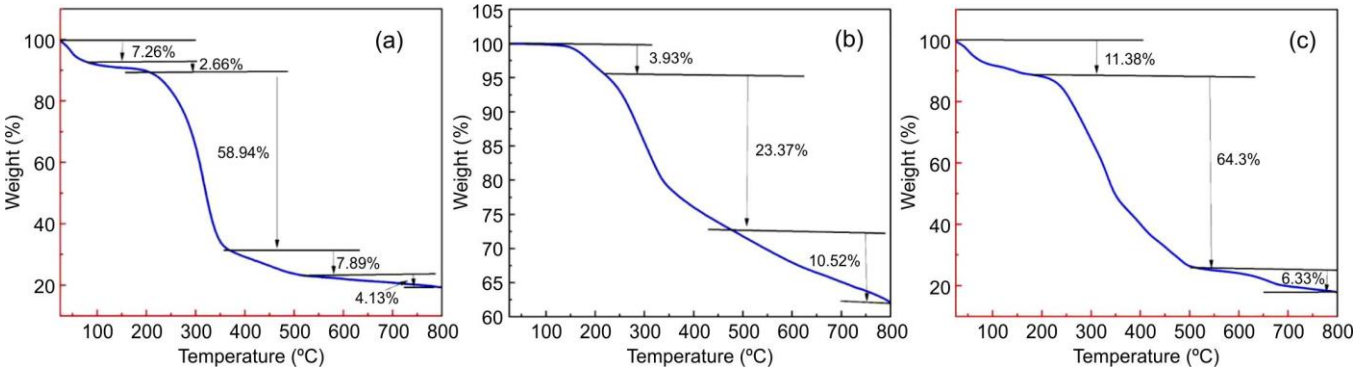

Fig. 4. Thermograms of (a) crude cellulose (b) α-cellulose and (c) β-cellulose

allow in-depth assessment of pyrolytic degradation mechanisms. For each model, the activation energy (E_a), pre-exponential factor (A) and regression coefficient (R^2) were calculated. The kinetic model that showed the strongest linear correlation was considered the most suitable. The kinetic study was performed within selected temperature ranges that correspond to the main mass-loss stages of cellulose decomposition. For crude cellulose, the analysis was performed over 190-360 ºC, while α-cellulose and β-cellulose were examined within 149-336 ºC and 240-518 ºC, respectively (Fig. 5a-c). These temperature ranges were selected to ensure reliable kinetic fitting by avoiding regions influenced by moisture loss and char formation.

As shown in Table-2, most of the reaction models used in the analysis achieved a high regression coefficient ($R^2 > 0.90$), indicating strong agreement with the experimental results. Among these, the DM-06 model based on the Zhuravlev equation gave the most accurate kinetic representation for crude cellulose. It produced the highest correlation regression coefficient ($R^2 = 0.973$), with an activation energy of 44.84×10^3 J mol^{-1} and a pre-exponential factor of 5.1×10^{-1} s^{-1}. The excellent linear fit (Fig. 6a) implies that under the selected pyrolysis conditions, crude cellulose degradation is governed by a diffusion-controlled reaction mechanism. For α-cellulose, the NM-4 kinetic model based on the Avrami-Erofeev equation (n = 2) was found to be the best fit (Fig. 6b). This model showed a very high regression coefficient of 0.986, along with an activation energy of 38.71×10^3 J mol^{-1} and frequency factor of 1.20 s^{-1}. The Avrami-Erofeev mechanism suggests that thermal degradation of α-cellulose is controlled by nucleation followed by growth processes, which is consistent with its more ordered crystalline structure.

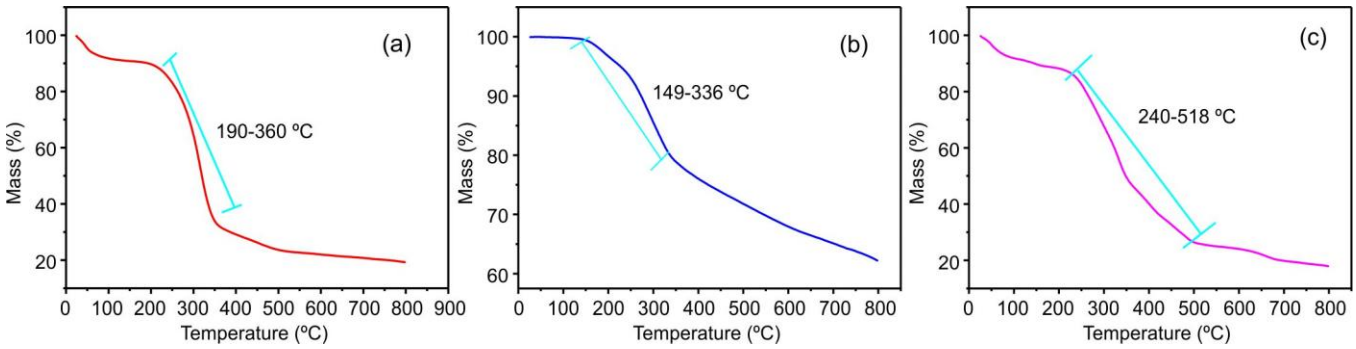

Fig. 5. Thermograms of (a) crude cellulose (b) α-cellulose and (c) β-cellulose at particular temperatures

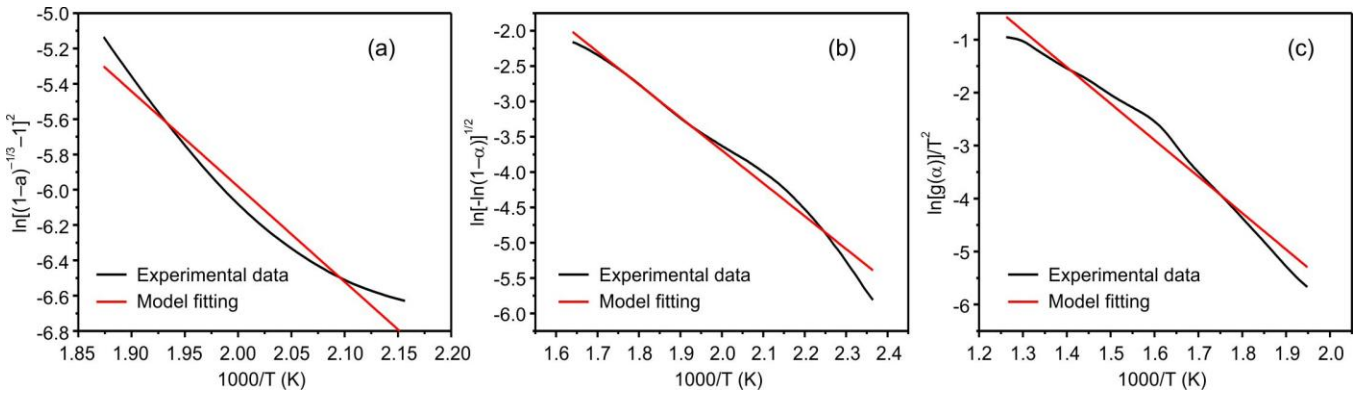

Fig. 6. Plots of applied kinetic models for (a) crude cellulose (b) α-cellulose and (c) β-cellulose

TABLE-2
KINETIC AND THERMODYNAMIC PARAMETERS DATA OF CELLULOSE CONTENTS

S. No.	Coats Redfern model of symbol	Type of Cellulose	Temperature range (ºC)	E_a (J mol^{-1}) × 10^3	A (s^{-1})	R^2	ΔS (J mol^{-1} K^{-1})	ΔH × 10^3 (J mol^{-1})	ΔG × 10^4 (J mol^{-1})
		Crude cellulose	190-360	30.77	1.80×10^{-1}	0.87	-262.18	24.24	22.15
1	CRO 0	α-cellulose	149-336	40.38	2.17	0.92	-247.35	36.27	22.72
		β-cellulose	240-518	41.52	1.92	0.92	-245.92	33.52	20.27
		Crude cellulose	190-360	50.62	2. 09 × 10	0.952	-215.79	46.11	21.20
2	CRO 1	α-cellulose	149-336	61.12	2.29×10^2	0.952	-209.51	53.02	20.56
		β-cellulose	240-518	66.78	6.97×10^2	0.953	-191.90	57.89	20.31
		Crude cellulose	190-360	77.83	3.00×10^4	0.969	-163.9	71.32	21.16
3	CRO 1.5	α-cellulose	149-336	119.37	2.30×10^9	0.93	-72.72	121.22	16.42
		β-cellulose	240-518	109.58	2.90×10^7	0.959	-111.56	101.46	18.98
		Crude cellulose	190-360	83.79	3.90×10^3	0.966	-116.25	75.40	21.61
4	CRO 2	α-cellulose	149-336	92.15	3.84×10^5	0.923	-147.15	84.10	21.22
		β-cellulose	240-518	87.40	1.65×10^5	0.962	-149.24	81.41	19.30
		Crude cellulose	190-360	87.83	1.80×10^5	0.969	-152.62	84.02	18.89
5	CRO 3	α-cellulose	149-336	131.24	1.70×10^{10}	0.87	-61.85	132.20	19.12
		β-cellulose	240-518	125.12	5.08×10^8	0.959	-85.75	12.88	18.89
		Crude cellulose	190-360	64.62	1.20×10^2	0.90	-214.26	58.86	21.96
6	DM 1	α-cellulose	149-336	82.87	7.21×10^3	0.936	-178.86	76.96	21.92
		β-cellulose	240-518	87.23	1.22×10^4	0.929	-171.02	79.62	21.16
		Crude cellulose	190-360	22.56	8.90×10^{-2}	0.92	-271.47	14.92	21.78
7	DM 2	α-cellulose	149-336	22.42	1.15×10^{-1}	0.91	-273.42	16.23	22.28
		β-cellulose	240-518	21.47	1.46×10^{-1}	0.942	-267.08	17.06	22.11
		Crude cellulose	190-360	102.92	8.90×10^5	0.959	-157.18	95.64	21.79
8	DM 3	α-cellulose	149-336	121.26	3.86×10^6	0.954	-123.66	113.84	21.79
		β-cellulose	240-518	124.64	8.54×10^6	0.968	-118.87	116.87	21.84
		Crude cellulose	190-360	74.89	6.23×10^1	0.92	-201.03	67.83	21.89
9	DM 4	α-cellulose	149-336	92.79	2.89×10^6	0.942	-164.66	87.08	21.08
		β-cellulose	240-518	97.21	7.09×10^4	0.932	-158.62	91.39	19.06
		Crude cellulose	190-360	87.96	1.90×10^3	0.91	-188.36	81.50	22.11
10	DM 5	α-cellulose	149-336	12.02	8.10×10^{-3}	0.945	-289.49	50.22	22.55
		β-cellulose	240-518	112.98	3.89×10^5	0.92	-143.98	106.68	22.65
		Crude cellulose	190-360	44.84	5.10×10^{-1}	0.973	-254.14	40.99	15.86
11	DM 6	α-cellulose	149-336	136.65	2.80×10^8	0.961	-92.02	132.43	18.87
		β-cellulose	240-518	57.34	1.49×10^1	0.98	-226.92	53.07	16.95
		Crude cellulose	190-360	87.12	1.96×10^3	0.942	-186.02	82.03	21.56
12	DM 7	α-cellulose	149-336	105.78	1.52×10^5	0.963	-153.23	99.65	20.89
		β-cellulose	240-518	107.20	1.86×10^5	0.956	-152.83	99.91	21.86
		Crude cellulose	190-360	79.06	2.98×10^2	0.927	-206.01	73.24	24.30
13	DM 8	α-cellulose	149-336	98.26	1.28×10^6	0.953	-171.02	91.34	20.96
		β-cellulose	240-518	96.96	1.39×10^4	0.94	-171.18	90.22	22.55
		Crude cellulose	190-360	8.9	1.64×10^{-3}	0.923	-317.89	2.83	24.37
14	GM 1	α-cellulose	149-336	50.72	7.80	0.952	-223.76	42.59	22.70
		β-cellulose	240-518	50.23	1.16	0.93	-231.40	43.77	22.62
		Crude cellulose	190-360	4.96	3.94×10^{-4}	0.93	-316.26	-1.29	23.78
15	GM 2	α-cellulose	149-336	53.24	1.31	0.952	-232.46	45.69	22.67
		β-cellulose	240-518	52.64	1.12	0.96	-221.79	48.87	22.64
		Crude cellulose	190-360	31.69	1.16×10^{-2}	0.90	-271.15	25.28	24.68
16	NM 1	α-cellulose	149-336	42.49	1.24	0.92	-251.56	39.66	21.25
		β-cellulose	240-518	42.56	1.89	0.93	-256.81	36.41	22.24
		Crude cellulose	190-360	34.67	6.70×10^{-2}	0.90	-269.21	27.24	23.23
17	NM 2	α-cellulose	149-336	41.40	0.689	0.929	-255.51	35.27	22.39
		β-cellulose	240-518	42.59	1.26	0.92	-249.21	36.27	22.89
		Crude cellulose	190-360	31.66	6.90×10^{-2}	0.92	-267.60	25.64	25.31
18	NM 3	α-cellulose	149-336	42.44	5.20×10^{-1}	0.94	-267.89	36.27	23.46
		β-cellulose	240-518	37.89	2.01×10^{-1}	0.932	-256.26	29.78	24.45

19	NM 4	Crude cellulose	190-360	44.98	3.70	0.948	-239.14	39.16	21.89
		α-cellulose	149-336	38.71	1.20	0.98642	-246.28	35.20	13.91
		β-cellulose	240-518	51.29	9.10×10^{1}	0.949	-226.52	44.78	21.45
20	NM 5	Crude cellulose	190-360	57.31	2.31	0.947	-256.38	38.75	22.54
		α-cellulose	149-336	61.12	6.30×10^{1}	0.97	-226.78	52.78	22.54
		β-cellulose	240-518	62.47	1.00×10^{2}	0.969	-215.12	56.75	22.64
21	NM 6	Crude cellulose	190-360	89.39	2.00×10^{4}	0.93	-169.82	88.78	22.89
		α-cellulose	149-336	119.10	1.70×10^{7}	0.968	-116.45	113.96	20.89
		β-cellulose	240-518	124.55	2.70×10^{7}	0.95	-115.52	120.49	20.06

In case of β-cellulose, the DM-06 model was again identified as the most suitable reaction mechanism (Fig. 6c). The model produced the highest regression coefficient (R^2 = 0.980), along with an activation energy of 57.34×10^3 J mol^{-1} and a relatively higher frequency factor of 1.49×10^{-1} s^{-1}. The higher activation energy indicates that β-cellulose has stronger hydrogen bonding and a more stable molecular structure compared to crude cellulose and β-cellulose. The relatively greater activation energy in the case of β-cellulose can be explained by the changes in the supramolecular structure; however, such factors as the crystallinity index, the degree of polymerisation and the intermolecular hydrogen bonding all have an impact on thermal stability and the degradation rate [25-27]. The activation energy values obtained for cellulose fall within the range of 120-240 kJ mol^{-1} reported for the cellulose derived from wood pulp, agricultural residues and cotton, depending on the source and analysis method, thereby supporting the reliability of the present results [27,28]. It is also worth to mention that differences in the activation energy among cellulose fractions arise from variations in crystallinity, molecular order and hydrogen bonding strength. Higher activation energy indicates greater thermal stability, while a larger frequency factor reflects increased molecular mobility and higher probability of reaction during pyrolysis.

Thermodynamic studies: Along with kinetic parameters, thermodynamic properties such as changes in (ΔH), entropy change (ΔS) and Gibb's free energy change (ΔG) were analysed. These parameters were calculated at a constant heating rate of 10 ºC min^{-1} using the same reaction model. The positive ΔH values obtained for all cellulose fractions indicate that the pyrolysis process is endothermic, meaning it needs a continuous supply of external heat to progress. For crude cellulose, the DM-06 model gave an enthalpy change (ΔH) value of 40.99×10^3 J mol^{-1}. In comparison, α-cellulose analysed using the NM-4 model showed a lower ΔH of 35.20×10^3 J mol^{-1}, suggesting that it requires less energy for decomposition. On the other hand, β-cellulose exhibited a much higher enthalpy change of 53.07×10^3 J mol^{-1}, which supports its higher resistance to thermal degradation. The Gibb's free energy change (ΔG) for all cellulose fractions was positive, with values between 1.39×10^5 to 1.70×10^5 J mol^{-1}. This indicates that pyrolytic degradation is not a spontaneous reaction and can occur only when heat is continuously supplied. In addition, the negative entropy (ΔS) implies a reduction in disorder during the process. This leads to the formation of solid char residues, indicating that the decomposition products have a more ordered structure compared to the original reactant. Thus, the kinetic and thermodynamic results indicate that cellulose pyrolysis follows the complex solid-state reaction pathways influenced by structural arrangement and hydrogen bonding. The agreement of the DM-06 and NM-4 models further highlights their suitability for describing the thermal degradation behaviour of different cellulose fractions.

Conclusion

Cellulose was successfully isolated from *Sericostoma pauciflorum* and fractionated into α- and β-cellulose. The structural and morphological analyses showed that α-cellulose possessed higher crystallinity and a more ordered structure, whereas β-cellulose was largely amorphous and formed aggregated particles. Thermal studies revealed distinct degradation behaviour among the fractions, with α-cellulose exhibiting the greatest thermal stability. Kinetic analysis using the Coats-Redfern approach revealed that the DM-06 model best explained the decomposition of crude cellulose and β-cellulose, whereas the NM-4 model was more appropriate for α-cellulose. The difference in activation energy values suggested variation in hydrogen bonding and molecular arrangement within the samples. Thermodynamic results confirmed that cellulose pyrolysis is an endothermic and non-spontaneous process that requires continuous energy supply.

ACKNOWLEDGEMENTS

The authors express their appreciation to the Department of Chemistry, Government College, Sirohi, India.

CONFLICT OF INTEREST

The authors declare that there is no conflict of interests regarding the publication of this article.

DECLARATION OF AI-ASSISTED TECHNOLOGIES

During the preparation of this manuscript, the authors used an AI-assisted tool(s) to improve the language. The authors reviewed and edited the content and take full responsibility for the published work.

REFERENCES

1. B.M. Sagar, M.M. Islam, M.L. Habib, S. Ahmed and M. Sahadat Hossain, *RSC Adv.*, **15**, 26276 (2025); https://doi.org/10.1039/D5RA02896E
2. E. Marinho, *Sustain. Chem. Environ.*, **11**, 100283 (2025); https://doi.org/10.1016/j.scenv.2025.100283

3. Y. Deng, T. Zhu, Y. Cheng, K. Zhao, Z. Meng, J. Huang, W. Cai and Y. Lai, *Adv. Fiber Mater.*, **6**, 1343 (2024); https://doi.org/10.1007/s42765-024-00454-0
4. M. Wohlert, T. Benselfelt, L. Wågberg, I. Furó, L.A. Berglund and J. Wohlert, *Cellulose*, **29**, 1 (2022); https://doi.org/10.1007/s10570-021-04325-4
5. H.M. Shaikh, R. Anis, A.M. Poulose, S.M. Al-Zahrani, N.A. Madhar, A. Alhamidi and M.A. Alam, *Polymers*, **13**, 1893 (2021); https://doi.org/10.3390/polym13111893
6. M. Kumar, P.S. Gehlot, D. Parihar, P.K. Surolia and G. Prasad, *Eur. Polym. J.*, **152**, 110448 (2021); https://doi.org/10.1016/j.eurpolymj.2021.110448
7. A.K. Siddhanta, K. Prasad, R. Meena, G. Prasad, G.K. Mehta, M.U. Chhatbar, M.D. Oza, S. Kumar and N.D. Sanandiya, *Bioresour. Technol.*, **100**, 6669 (2009); https://doi.org/10.1016/j.biortech.2009.07.047
8. T. Garg, S. Arora and R. Pahwa, *Future J. Pharm. Sci.*, **11**, 76 (2025); https://doi.org/10.1186/s43094-025-00834-2
9. G. Chang, S. Dai, X. Ye, J. Li, Y. Ren, W. Cui, C. Wang and J. Zhang, *Sustain. Energy Fuels*, **9**, 3721 (2025); https://doi.org/10.1039/D5SE00486A
10. H. Zhou, Y. Long, A. Meng, S. Chen, Q. Li and Y. Zhang, *RSC Adv.*, **5**, 26509 (2015); https://doi.org/10.1039/C5RA02715B
11. M. Choudhary, S. Kumar Jain, D. Singh, K. Srivastava, A.K. Patel, J. Mahlknecht, B. Shekher Giri and M. Kumar, *Bioresour. Technol.*, **380**, 129065 (2023); https://doi.org/10.1016/j.biortech.2023.129065
12. O. Fischer, R. Lemaire and A. Bensakhria, *J. Therm. Anal. Calorim.*, **149**, 10941 (2024); https://doi.org/10.1007/s10973-023-12868-w
13. C. Zheng, D. Li and M. Ek, *J. Therm. Anal. Calorim.*, **135**, 3015 (2019); https://doi.org/10.1007/s10973-018-7564-5
14. J. Cai, W. Wu, R. Liu and G.W. Huber, *Green Chem.*, **15**, 1331 (2013); https://doi.org/10.1039/c3gc36958g
15. M. Raza, B. Abu-jdayil, A.H. Al-marzouqi and A. Inayat, *Renew. Energy*, **183**, 67 (2022); https://doi.org/10.1016/j.renene.2021.10.065
16. O. Bongomin, C. Nzila, J. Igadwa Mwasiagi and O. Maube, *Energy Convers. Manag. X*, **24**, 100723 (2024); https://doi.org/10.1016/j.ecmx.2024.100723
17. M. Raza, B. Abu-Jdayil and A. Inayat, *Fuel*, **342**, 127799 (2023); https://doi.org/10.1016/j.fuel.2023.127799
18. M. Raza and B. Abu-Jdayil, *Case Stud. Therm. Eng.*, **47**, 103118 (2023); https://doi.org/10.1016/j.csite.2023.103118
19. G. Singh, R.K. Mishra and N. Kumar, *RSC Adv.*, **15**, 43487 (2025); https://doi.org/10.1039/D5RA06424D
20. D. Parihar, M. Kumar, P.S. Gehlot, P.K. Surolia and G. Prasad, *J. Nat. Fibers*, **19**, 10499 (2021); https://doi.org/10.1080/15440478.2021.1994092
21. M. Raza, B. Abu-Jdayil, F. Banat and A.H. Al-Marzouqi, *ACS Omega*, **7**, 25366 (2022); https://doi.org/10.1021/acsomega.2c02333
22. M. Uddin Monir, S. Muntasir Shovon, F. Ahamed Akash, M.A. Habib, K. Techato, A. Abd Aziz, S. Chowdhury and T.A. Eka Prasetya, *Case Stud. Therm. Eng.*, **55**, 104186 (2024); https://doi.org/10.1016/j.csite.2024.104186
23. X.-Q. Wu, P.-D. Liu, Q. Liu, S.-Y. Xu, Y.-C. Zhang, W.-R. Xu and G.-D. Liu, *RSC Advances*, **11**, 14071 (2021); https://doi.org/10.1039/D1RA02259H
24. H.S. Hafid, F.N. Omar, E.K. Bahrin and M. Wakisaka, *Bioresour. Bioprocess.*, **10**, 7 (2023); https://doi.org/10.1186/s40643-023-00631-w
25. S. Zhang, J. Li, H. Niu, W. Xu, J. Xu, W. Hu and X. Wang, *ChemPlusChem*, **78**, 192 (2013); https://doi.org/10.1002/cplu.201200272
26. A. Hayat, F. Raziq, M. Khan, I. Ullah, M. Ur Rahman, W.U. Khan, J. Khan and A. Ahmad, *J. Photochem. Photobiol. Chem.*, **379**, 88 (2019); https://doi.org/10.1016/j.jphotochem.2019.05.011
27. A.K. Burnham, X. Zhou and L.J. Broadbelt, *Energy Fuels*, **29**, 2906 (2015); https://doi.org/10.1021/acs.energyfuels.5b00350
28. Y. Liang, M.E. Ries and P.J. Hine, *Carbohydr. Polym.*, **305**, 120518 (2023); https://doi.org/10.1016/j.carbpol.2022.120518